

Voltage-dependent spin flip in magnetically substituted graphene nanoribbons: Towards the realization of graphene-based spintronic devices

Gregory Houchins,¹ Charles B. Crook,¹ Jian-Xin Zhu,^{2,3} Alexander V. Balatsky,^{4,5} and Jason T. Haraldsen^{1,6,*}

¹*Department of Physics and Astronomy, James Madison University, Harrisonburg, Virginia 22802, USA*

²*Theoretical Division, Los Alamos National Laboratory, Los Alamos, New Mexico 87545, USA*

³*Center for Integrated Nanotechnologies, Los Alamos National Laboratory, Los Alamos, New Mexico 87545, USA*

⁴*Institute for Materials Science, Los Alamos National Laboratory, Los Alamos, New Mexico 87545, USA*

⁵*NORDITA, Roslagstullsbacken 23, 106 91 Stockholm, Sweden*

⁶*Department of Physics, University of North Florida, Jacksonville, Florida 32224, USA*

(Received 17 May 2016; revised manuscript received 6 April 2017; published 28 April 2017)

We examine the possibility of using graphene nanoribbons (GNRs) with directly substituted chromium atoms as a spintronic device. Using density functional theory, we simulate a voltage bias across a constructed GNR in a device setup where a magnetic dimer has been substituted into the lattice. Through this first-principles approach, we calculate the electronic and magnetic properties as a function of Hubbard U , voltage, and magnetic configurations. By calculating the total energy of each magnetic configuration, we determine that the initial antiferromagnetic ground state flips to a ferromagnetic state with applied bias. Mapping this transition point to the calculated conductance for the system reveals that there is a distinct change in conductance through the GNR, which indicates the possibility of a spin valve. We also show that this corresponds to a distinct shift in the induced magnetization within graphene.

DOI: [10.1103/PhysRevB.95.155450](https://doi.org/10.1103/PhysRevB.95.155450)

I. INTRODUCTION

Over the past couple of decades, solid-state research has guided the advancement of technologies, which includes the control and manipulation of charge transport in various materials. Progress in the overall understanding of electronic systems has led to the development of p - n junctions, giant and colossal magnetoresistance, and the whole realm of semiconductor physics, for which today's technology is based. Currently, the vast majority of these technologies take advantage of only the charge degree of freedom in materials. However, over the past two decades, there has been a significant push to combine the electronic and spin degrees of freedom in both multiferroic materials and spintronic devices [1–3]. These endeavors have ranged from molecular spintronics [4–6] to quantum dot systems [7] to topological insulators [8] where a major motivation is the realization and enhancement of quantum computation and nanotechnology [9–11].

Recently, graphene has gained a large amount of experimental and theoretical attention due to its distinct electron mobility produced through carbon-carbon (C-C) π bonding that enables an electron delocalization throughout its honeycomb lattice structure [12–16]. Due to the presence of a Dirac cone in the electronic structure, graphene is known as a Dirac material [17]. Therefore, the presence of a Dirac cone allows graphene to be classified as both a zero-gap semiconductor and a zero density of states (DOS) metal [12,18], which means that the electrons have the characteristics of ultrarelativistic massless particles [19]. Furthermore, graphene also exhibits enhanced thermal and tensile strength properties [20–22].

Besides the well-known electronic and thermal properties of graphene, it has been shown that graphene can obtain distinct magnetic properties through the addition of adatoms

placed on the lattice through the placement of graphene on a substrate (e.g., yttrium iron garnet) and through various other interactions [23–31]. Recently, it was shown that the direct substitution of magnetic impurities into the graphene lattice also could induce localized magnetism that interacts through the conduction electrons in graphene [32,33]. Furthermore, this paper along with others have detailed the potential for using graphene substitution as spintronic transistors, spin valves, and other devices [34,35].

In our previous computational work [33], the presence of two transition-metal atoms in graphene produced a distinct induction of magnetism in local carbon atoms where it was shown that the spatial effect of two magnetic impurities produced Ruderman-Kittel-Kasuya-Yosida (RKKY) interactions through the conduction electrons that culminated in either ferromagnetic (FM) or antiferromagnetic (AFM) ground states [36–39]. Here, the ability to induce magnetism through a RKKY interaction indicates a high potential for the use of a transition-metal substituted graphene nanoribbon (GNR) as a possible spintronic device. Although the use of GNRs as a spintronic device has been demonstrated in various studies [34,35,40–42], these studies mainly have focused on the utilization of magnetic edge states in the GNR. Therefore, it is proposed that direct substitution of the magnetic atoms may provide better control and handling of the spin states through an applied voltage coupling to the RKKY interactions.

In this paper, we explore the possibility of controlling the magnetic states generated by two chromium (Cr) atoms substituted into graphene through the use of an applied bias voltage. Using density functional theory through a generalized gradient approximation (GGA), we simulated a spintronic device made from a GNR with two chromium atoms substituted into the lattice. By calculating multiple magnetic configurations using a varying on-site potential and applied voltage bias, we determined the device density of states, magnetic profile, and voltage dependence for these spintronic devices. Furthermore,

*Corresponding author. j.t.haraldsen@unf.edu

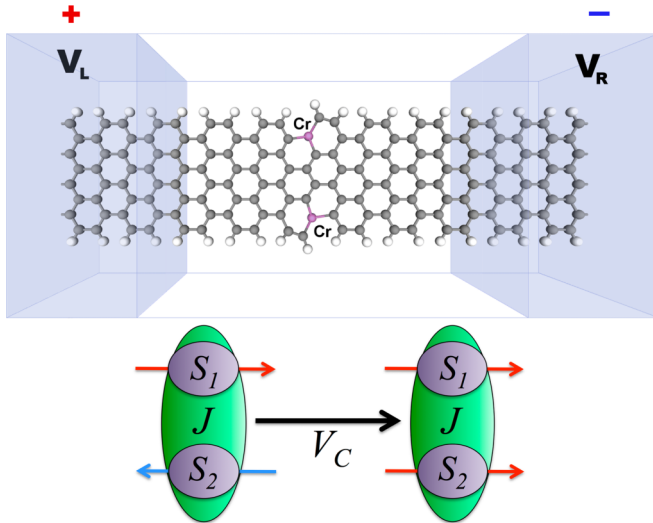


FIG. 1. A GNR device setup between two electrodes. The voltage between the two electrodes is varied by giving the left electrode a positive charge and the right a negative charge each equal in magnitude to half the total potential difference desired. The graphene is doped with two chromium atoms separated by four carbons. At a critical voltage V_c , the spin ground state flips from antiferromagnetic to ferromagnetic.

we examine the conductivity of the GNR and show that, as the nanoribbon crosses a critical voltage, the magnetic ground state flips from antiferromagnetic to ferromagnetic, which produces a distinct change in the induced magnetism of graphene and the overall conductance. This paper provides a theoretical realization of a graphene-based spintronic device and will hopefully motivate experimental endeavors in this direction.

II. COMPUTATIONAL METHODS

This paper presents first-principles calculations of electron interactions throughout a magnetically doped GNR device. To simulate a spin switch device, we constructed a GNR ($10.4 \times 22.7 \text{ \AA}^2$) with 0.710-nm electrodes on each side consisting of 120 total atoms. The electrodes are used to simulate a voltage bias across the device. In the center of the GNR, two of the carbons were replaced by chromium atoms where the chromium atoms were separated by four carbon atoms along the zigzag chain direction. To assure a nanoribbon configuration, the dangling bonds of the edge carbons are capped with hydrogen (illustrated in Fig. 1).

Using the density functional codes of the ATOMISTIC TOOLKIT [43], we performed a geometry optimization on a supercell of graphene to obtain the required distortion using a 5×5 k -point optimization in two dimensions. This optimization allowed us to obtain the known graphene impurity distortion shown by Crook *et al.* [33]. Once the geometry was determined precisely, the supercell was converted into a two-point probe, and the distortion was kept constant to reduce computational time for the device setup. The electronic structure then was optimized using a spin-polarized generalized gradient approximation (SGGA) with a Hubbard on-site potential using Perdew, Burke, and Ernzerhof (PBE) functionals [44–46]. Calculations were performed for various

on-site potential U 's (0–4 eV), voltage biases (0, 0.25, 0.5, 0.75, and 1 V), and $1 \times 1 \times 5$ k -point mesh for the nanoribbon ($1 \times 1 \times 100$ k -point mesh for the electrodes). The overall magnetic ground state for each set of parameters was determined by comparing the total energy for a ferromagnetic and antiferromagnetic configuration. To assure consistency between magnetic ground states, we used a tolerance of 0.3 meV for the total energy convergence. Furthermore, to examine the electronic and magnetic properties, we calculated the device density of states, magnetic moment, and conductance.

III. ANTIFERROMAGNETIC/FERROMAGNETIC SPIN FLIP

In a previous study, it was shown that the magnetic interactions between chromium atoms in graphene interact through an induction of magnetism in carbon and couple through the carbon conduction electrons [33]. This indicated that there might be the potential to affect the magnetic states through the use of an external electric field or applied voltage. Therefore, this paper presents the results from a device setup to show that two Cr atoms in a GNR may have the ability to produce spin switch, which opens the possibility for creating a spintronic device using magnetically doped graphene.

To create a spin interaction, two chromium atoms are placed in the GNR along the zigzag direction with a spacing of four carbon atoms. ΔE is determined by comparing the calculated total energy for the antiferromagnetic ($\uparrow\downarrow$) and ferromagnetic ($\uparrow\uparrow$) Cr-Cr configurations. To model this system, we consider a classical dimer with a Hamiltonian given by

$$H = -\frac{J}{2} \vec{S}_1 \cdot \vec{S}_2, \quad (1)$$

where J is the superexchange energy ($J > 0$ for FM and $J < 0$ for AFM) and S is the spin [47]. This allows us to evaluate the classical energy as

$$E = -\frac{JS^2}{2} \cos(\theta_1 - \theta_2), \quad (2)$$

where $\theta = 0^\circ$ or 180° for up or down spins, respectively. A general θ can be used for frustrated or canted spins [48]. From this, $E_{\text{FM}} = -JS^2/2$ and $E_{\text{AFM}} = JS^2/2$, which makes $\Delta E = JS^2$. Therefore, the change in energy is directly related to the Cr-Cr dimer superexchange energy. It should be noted that this is a generalization since the induction of magnetic moments in the nearby carbon atoms will produce a magnetic “dumbbell.” However, the size of the induced moment is small and will only provide a small perturbation of the original Hamiltonian.

As shown in Fig. 2(a), the zero-bias magnetic ground state for the device setup is determined to be antiferromagnetic, which is consistent with the bulk supercell calculations from Ref. [33]. Furthermore, as the applied voltage bias across the device is increased, there is a distinct change in the magnetic ground state at $V_c = 0.37$ V where the ground state is shifted to a ferromagnetic state.

At the same critical voltage, we find that conductance shows a dramatic increase throughout the GNR [Fig. 2(b)] while producing an overall drop in the average magnetic moment in carbon [Fig. 2(c)]. Interestingly, the critical voltage remains

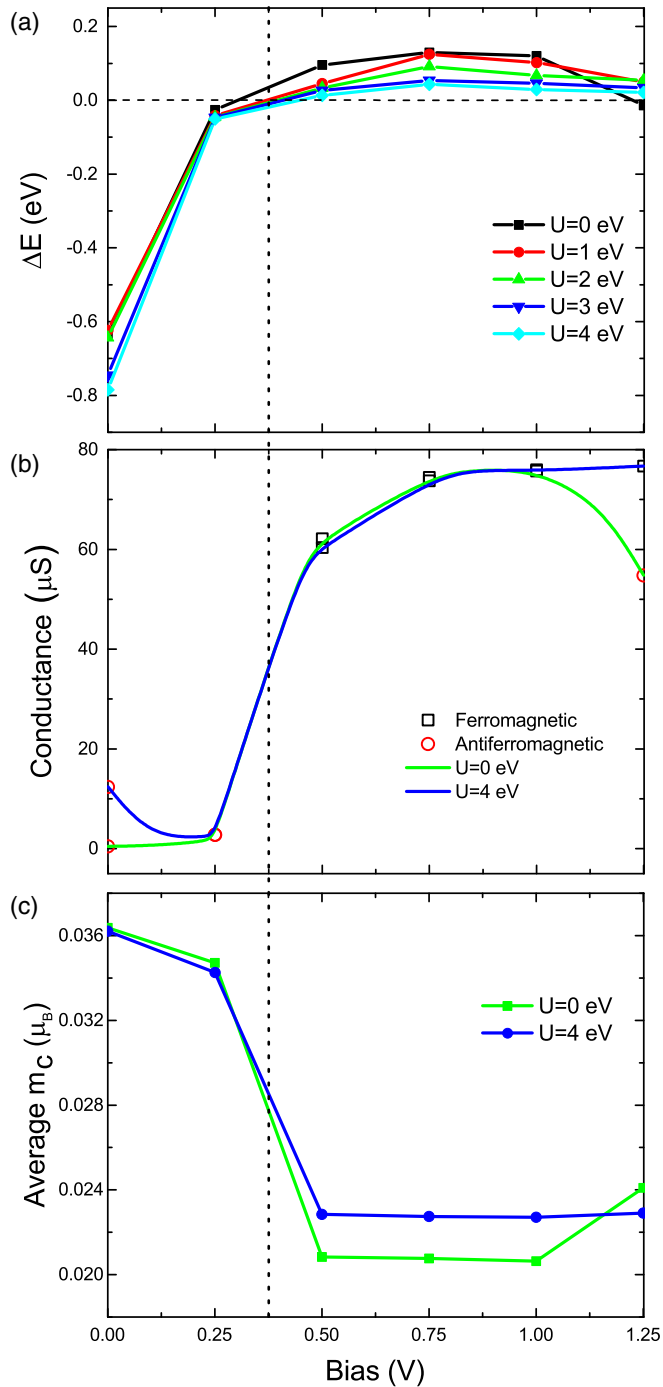


FIG. 2. (a) The difference in total energy of the two Cr spin orientation states. Here, the difference is taken to be $\uparrow\downarrow - \uparrow\uparrow$, therefore a positive difference denotes a spin $\uparrow\uparrow$ ground state. This difference is shown for various Hubbard U 's varying from 0 eV to a maximum of 4 eV. (b) The calculated conductance of the GNR device as a function of bias for both $U = 0$ and $U = 4$ eV. (c) The average of the absolute value of the magnetic moment of all the carbon atoms as a function of bias for a Hubbard U of 0 and 4 eV. There is a vertical dotted line at 0.375 V to show the same point of change in characteristics from AFM to FM in all three graphs.

constant regardless of the assumed on-site Hubbard U . As the voltage further increases, the simulation of the $U = 0$ eV device oscillates back to an antiferromagnetic ground state,

which could be indicative of the interaction between the conduction electrons and the voltage bias that produces a voltage-dependent interaction as observed in Ref. [40]. However, as the on-site potential is increased, the overall oscillatory nature is reduced and practically levels out, which provides a potential experimental verification point for the spin-flip nature.

For the $U = 0$ calculations, the conductance drops again around 1.25 eV, which indicates that this phenomenon may be dependent on the AFM state. The low conductance in the AFM state below the critical voltage is consistent with a magnetoresistance device. Therefore, the use of conductance could be used to determine that a spin flip has occurred. From these calculations, there is a threshold of about 60 μS indicating a transition from AFM to FM.

IV. THE DEVICE DENSITY OF STATES

The shift in the magnetic state indicates that, as the voltage is increased, the electrons used to produce the antiferromagnetic interaction are elevated into the conduction band. This is shown in the calculated DOS (shown in Fig. 3) where the change in the electronic structure shifts the magnetic interaction between the chromium atoms and produces a ferromagnetic ground-state configuration. Figure 3(a) shows the calculated local DOS for both the Cr and the C sites at both 0 and 1 V for a Hubbard U of 0 eV [Fig. 3(b) shows $U = 4.0$ eV]. A comparison of the projected DOS for both $U = 0$ and 4 eV (shown in Fig. 4) shows that this effect is produced regardless of an on-site potential. When the density of states of the device has zero bias, there are clearly no states at the Fermi level and therefore no conduction. This changes as one increases the on-site potential. However, at a bias of 1.0 V, this behavior changes as the number of states at the Fermi level rises.

If we look at the local density of states for just one chromium atom, we see a similar pattern of no states at the Fermi level without a bias present, and then states become present when the bias is added. This means that the conduction of graphene increases as the voltage increases, which is supported by the calculated conductance of the device at each bias. There is a direct correlation of conductance and magnetic ordering as seen in Fig. 2 indicating that the increased conductance is producing the flip in the exchange interaction between the chromium atoms. We can see similar patterns in the local density of states for the carbon. However, the number of states are about an order of magnitude less than that of Cr.

V. MAGNETIZATION MAPPING

In Fig. 5, we determine the magnetic moment as a function of the atomic spacing throughout the simulated GNR along with varying voltage and on-site potential. The first two columns show a consistent AFM configuration for the Cr-Cr dimers. However, it is clear that a distinct magnetization is drawn into the nearest-neighbor carbon atoms, which has shown a proximity induced magnetization of graphene in Ref. [33]. The magnetic moment on the Cr atoms appears to be $> 3.6\mu_B$ where the additional magnetization of carbon lowers the overall magnetic moment per Cr atom to about $2\mu_B$.

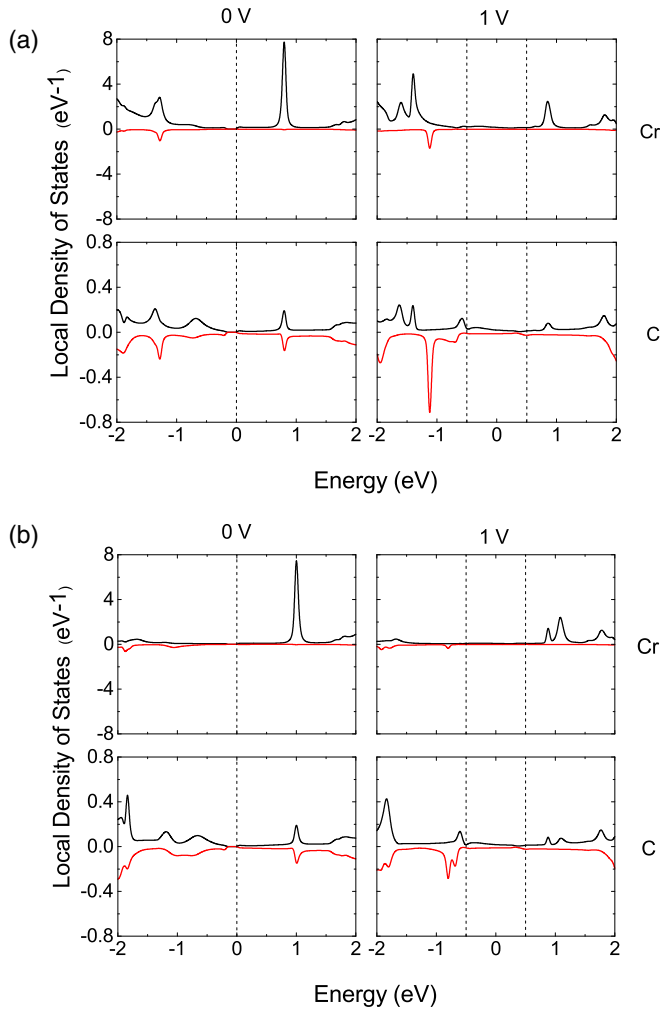


FIG. 3. The local density of states (LDOS) for chromium and carbon with Hubbard U 's of (a) $U = 0$ eV and (b) $U = 4$ eV for a bias of 0 and 1 V each. The black line denotes the spin-up electron states, whereas the red line denotes spin down. The dotted lines indicate the Fermi levels of the device. Note, in the case of a 1-V bias, there are two Fermi levels at -0.5 and 0.5 eV due to the bias. The atoms used for this figure are the top Cr atom and the second carbon atom down from that Cr with respect to the orientation seen in Fig. 1.

These values are in slight disagreement with the findings of Refs. [25,26]. However, this could be due to the configuration and/or type of calculation used. Since the spin-flip effect is independent of the local magnetic moment, the slight difference is inconsequential.

Furthermore, the induction of magnetic moment on the carbon atoms is reduced slightly with the increasing on-site potential, which is shown as an increase in the Cr magnetic moment as a function of U in Fig. 6. As the applied voltage is increased to the critical threshold of 0.37 V, there is a dramatic shift in the magnetization profile as conductance is increased and the Cr-Cr dimer transitions to a FM state. There is also a shift in the magnetic moment of carbon [shown in Fig. 2(c)].

The decrease in magnetization in the FM states implies that the magnetization is related inversely to conductance where the largest decline in magnetic moment is in the two

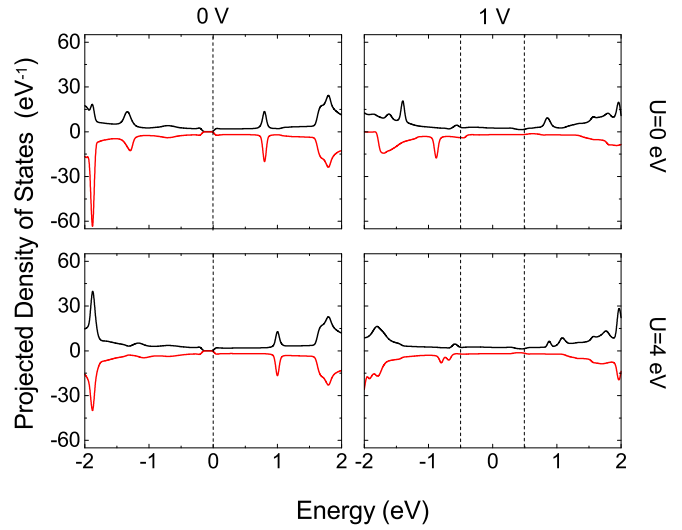


FIG. 4. The projected density of states for a bias of 0 and 1 V both in the case of Hubbard U 's of 0 and 4 eV. Again, the black denotes spin up, and the red denotes spin down. The Fermi levels are again shown with dotted lines.

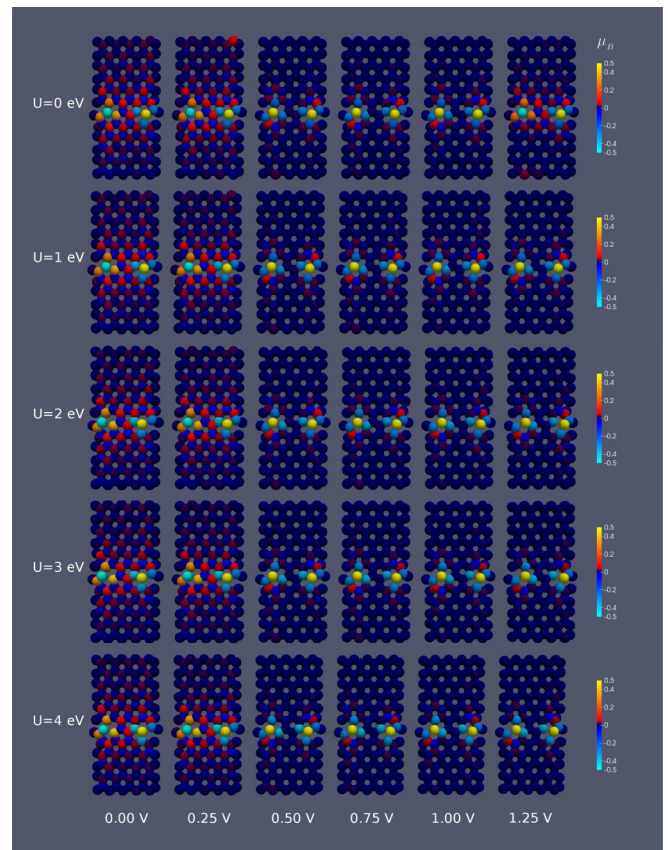


FIG. 5. Magnetic moment for each atom in the GNR device for various biases and Hubbard U 's. The scale has been renormalized between $-0.5\mu_B$ and $0.5\mu_B$ to show the magnetization of the carbon atoms around the chromium atoms in more detail. The magnetic moment on the Cr atoms varies from 3.6 to $4.0\mu_B$ depending on the Hubbard U as seen in Fig. 6.

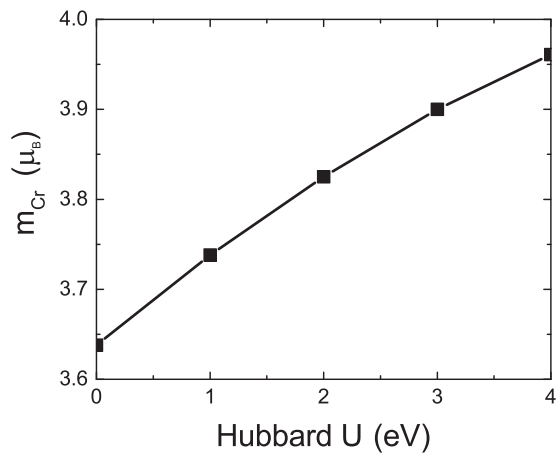


FIG. 6. The magnetic moment for the Cr atoms as a function of Hubbard U . For simplicity the magnetic moment of Cr in the case of no bias was used since the magnetic moment varied little with respect to bias.

middle carbons between the Cr atoms. This seems to be produced by the shift in conductance which is affected by the voltage-dependent magnetic interaction and supports the conclusion that conduction electrons mediate through a RKKY interaction [36–38].

Therefore, regardless of magnetic moment on the carbon and/or Cr atoms, the spin flip occurs at the same critical voltage. This change in magnetic state (AFM \rightarrow FM) is occupied by a distinct drop in magnetization in the middle carbon atoms produced by the increase in conduction of the graphene sheet.

VI. CONCLUSIONS

Overall, we examine the voltage dependence of a magnetically substituted GNR device and show that the magnetic interactions change with applied voltage strength. Based on an analysis of the projected DOS and the conductivity, it

appears that the coupling interaction between the Cr atoms is competing with the conduction electrons that contribute to antiferromagnetic ordering. Once the critical voltage is reached, the magnetic coupling between the Cr atoms flips into an overall FM interaction. This changes the magnetic induction within the GNR where it is changed effectively from AFM to FM. As shown in Ref. [33], the FM state allows for a greater conduction of the carbon atoms (shown by the LDOS in Fig. 3). Therefore, the overall conductance is increased by a few orders of magnitude.

The dramatic change in the conductance of the device at the same critical voltage for which there is a change in the magnetic state of the chromium atoms allows one to resolve the magnetic phase and to employ this effect in prospective graphene-based nanospintronic devices. This correlation is supported by the apparent decrease in conductance when the $U = 0$ eV case flips back to the AFM ground state. Essentially, the AFM ground state forces the carbon atoms into an induced AFM state, which reduces the conductance by producing a correlation barrier. Once the GNR is changed into the FM state, the correlation barrier is reduced or eliminated.

In closing, this paper shows the potential for GNRs to be utilized as spintronic devices with direct magnetic substitutions. It is the goal of this research to motivate experimental endeavors in this direction.

ACKNOWLEDGMENTS

This work was supported by U.S. DOE Basic Energy Sciences Grant No. E304. G.H., C.B.C., and J.T.H. acknowledge undergraduate support from the Institute for Materials Science at Los Alamos National Laboratory. J.T.H. acknowledges computational support provided by the Center for Integrated Nanotechnologies. The work at Los Alamos National Laboratory was carried out under the auspices of the U.S. DOE and NNSA under Contract No. DEAC52-06NA25396 and supported by the U.S. DOE Basic Energy Sciences Office (J.-X.Z. and A.V.B.).

-
- [1] S. A. Wolf *et al.*, Spintronics: A spin-based electronics vision for the future, *Science* **294**, 1488 (2001).
 - [2] S. D. Bader and S. S. P. Parkin, Spintronics, *Annu. Rev. Condens. Matter Phys.* **1**, 71 (2010).
 - [3] I. Zutic, J. Fabian, and S. Das Sarma, Spintronics: Fundamentals and applications, *Rev. Mod. Phys.* **76**, 323 (2004).
 - [4] A. R. Rocha *et al.*, Towards molecular spintronics, *Nat. Mater.* **4**, 335 (2005).
 - [5] L. Bogani and W. Wernsdorfer, Molecular spintronics using single-molecule magnets, *Nat. Mater.* **7**, 179 (2008).
 - [6] A. A. Khajetoorians, J. Wiebe, B. Chilian, and R. Wiesendanger, Realizing all-spin-based logic operations atom by atom, *Science* **332**, 1062 (2011).
 - [7] H.-A. Engel, P. Recher, and D. Loss, Electron spins in quantum dots for spintronics and quantum computation, *Solid State Commun.* **119**, 229 (2001).
 - [8] D. Pesin and A. H. MacDonald, Spintronics and pseudospintronics in graphene and topological insulators, *Nat. Mater.* **11**, 409 (2012).
 - [9] D. Awschalom, D. Loss, and N. Samarth, *Semiconductor Spintronics and Quantum Computation* (Springer Science & Business Media, Berlin, 2002).
 - [10] Y. Matsumoto *et al.*, Combinatorial investigation of spintronic materials, *MRS Bull.* **28**, 734 (2003).
 - [11] Y. Xu and S. Thompson, *Spintronic Materials and Technology* (CRC Press, Boca Raton, FL, 2007).
 - [12] A. K. Geim and K. S. Novoselov, The rise of graphene, *Nat. Mater.* **6**, 183 (2007).
 - [13] A. H. Castro Neto *et al.*, The electronic properties of graphene, *Rev. Mod. Phys.* **81**, 109 (2009).
 - [14] J.-H. Chen, C. Jang, S. Xiao, M. Ishigami, and M. S. Fuhrer, Intrinsic and extrinsic performance limits of graphene devices on SiO₂, *Nat. Nanotechnol.* **3**, 206 (2008).
 - [15] E. Pop, V. Varshney, and A. K. Roy, Thermal properties of graphene: Fundamentals and applications, *MRS Bull.* **37**, 1273 (2012).
 - [16] K. I. Bolotin *et al.*, Ultrahigh electron mobility in suspended graphene, *Solid State Commun.* **146**, 351 (2008).

- [17] T. O. Wehling, A. M. Black-Schaffer, and A. V. Balatsky, Dirac materials, *Adv. Phys.* **63**, 1 (2014).
- [18] K. S. Novoselov *et al.*, Two-dimensional gas of massless Dirac fermions in graphene, *Nature (London)* **438**, 197 (2005).
- [19] M. Müller, J. Schmalian, and L. Fritz, Graphene: A Nearly Perfect Fluid, *Phys. Rev. Lett.* **103**, 025301 (2009).
- [20] S. V. Morozov, K. S. Novoselov, M. I. Katsnelson, F. Schedin, D. C. Elias, J. A. Jaszczak, and A. K. Geim, Giant Intrinsic Carrier Mobilities in Graphene and Its Bilayer, *Phys. Rev. Lett.* **100**, 016602 (2008).
- [21] A. A. Balandin *et al.*, Superior thermal conductivity of single-layer graphene, *Nano Lett.* **8**, 902 (2008).
- [22] Y. Zhu *et al.*, Graphene and graphene oxide: Synthesis, properties, and applications, *Adv. Mater.* **22**, 3906 (2010).
- [23] O. V. Yazyev and M. I. Katsnelson, Magnetic Correlations at Graphene Edges: Basis for Novel Spintronics Devices, *Phys. Rev. Lett.* **100**, 047209 (2008).
- [24] C. N. R. Rao, H. S. S. R. Matte, K. S. Subrahmanyam, and U. Maitra, Unusual magnetic properties of graphene and related materials, *Chem. Sci.* **3**, 45 (2012).
- [25] A. V. Krasheninnikov, P. O. Lehtinen, A. S. Foster, P. Pyykkö, and R. M. Nieminen, Embedding Transition-Metal Atoms in Graphene: Structure, Bonding, and Magnetism, *Phys. Rev. Lett.* **102**, 126807 (2009).
- [26] E. J. G. Santos, A. Ayuela, and D. Sanchez-Portal, First-principles study of substitutional metal impurities in graphene: structural, electronic and magnetic properties, *New J. Phys.* **12**, 053012 (2010).
- [27] F. M. Hu, T. Ma, H.-Q. Lin, and J. E. Gubernatis, Magnetic impurities in graphene, *Phys. Rev. B* **84**, 075414 (2011).
- [28] Z. Wang, C. Tang, R. Sachs, Y. Barlas, and J. Shi, Proximity-Induced Ferromagnetism in Graphene Revealed by the Anomalous Hall Effect, *Phys. Rev. Lett.* **114**, 016603 (2015).
- [29] H. Wang, Doping monolayer graphene with single atom substitutions, *Nano Lett.* **12**, 141 (2012).
- [30] R. Lv *et al.*, Nitrogen-doped graphene: beyond single substitution and enhanced molecular sensing, *Sci. Rep.* **2**, 586 (2012).
- [31] V. K. Dugaev, V. I. Litvinov, and J. Barnas, Exchange interaction of magnetic impurities in graphene, *Phys. Rev. B* **74**, 224438 (2006).
- [32] D. W. Boukhvalov, M. I. Katsnelson, and A. I. Lichtenstein, Hydrogen on graphene: Electronic structure, total energy, structural distortions and magnetism from first-principles calculations, *Phys. Rev. B* **77**, 035427 (2008).
- [33] C. B. Crook, C. Constantin, T. Ahmed, J.-X. Zhu, A. V. Balatsky, and J. T. Haraldsen, Proximity-induced magnetism in transition-metal substituted graphene, *Sci. Rep.* **5**, 12322 (2015).
- [34] W. X. Zhang, Voltage-driven spintronic logic gates in graphene nanoribbons, *Sci. Rep.* **4**, 6320 (2014).
- [35] Q. Q. Sun *et al.*, Atomic scale investigation of a graphene nanoribbon based high efficiency spin valve, *Sci. Rep.* **3**, 2921 (2013).
- [36] M. A. Ruderman and C. Kittel, Indirect exchange coupling of nuclear magnetic moments by conduction electrons, *Phys. Rev.* **96**, 99 (1954).
- [37] T. A. Kasuya, Theory of metallic ferro- and antiferromagnetism on zeneros model, *Prog. Theor. Phys.* **16**, 45 (1956).
- [38] K. Yosida, Magnetic properties of Cu-Mn alloys, *Phys. Rev.* **106**, 893 (1957).
- [39] M. Sherafati and S. Satpathy, RKKY interaction in graphene from the lattice Green's function, *Phys. Rev. B* **83**, 165425 (2011).
- [40] P. M. Haney, C. Heiliger, and M. D. Stiles, Bias dependence of magnetic exchange interactions: Application to interlayer exchange coupling in spin valves, *Phys. Rev. B* **79**, 054405 (2009).
- [41] Y.-C. Lin, P.-Y. Teng, P.-W. Chiu, and K. Suenaga, Exploring the Single Atom Spin State by Electron Spectroscopy, *Phys. Rev. Lett.* **115**, 206803 (2015).
- [42] X. Hu, N. Wan, L. Sunand, and A. V. Krasheninnikov, Semiconductor to metal to half-metal transition in Pt-embedded zigzag graphene nanoribbons, *J. Phys. Chem. C* **118**, 16133 (2014).
- [43] ATOMISTIC TOOLKIT version 13.8, QuantumWise A/S, <http://www.quantumwise.com>.
- [44] M. Brandbyge, J.-L. Mozos, P. Ordejón, J. Taylor, and K. Stokbro, Density-functional method for nonequilibrium electron transport, *Phys. Rev. B* **65**, 165401 (2002).
- [45] J. M. Soler *et al.*, The SIESTA method for ab initio order-N materials simulation, *J. Phys.: Condens. Matter* **14**, 2745 (2002).
- [46] J. P. Perdew, K. Burke, and M. Ernzerhof, Generalized Gradient Approximation Made Simple, *Phys. Rev. Lett.* **77**, 3865 (1996).
- [47] J. T. Haraldsen, T. Barnes, and J. L. Musfeldt, Neutron scattering and magnetic observables for $S=1/2$ spin clusters and molecular magnets, *Phys. Rev. B* **71**, 064403 (2005).
- [48] J. T. Haraldsen and R. S. Fishman, Spin rotation technique for non-collinear magnetic systems: Application to the generalized Villain model, *J. Phys.: Condens. Matter* **21**, 216001 (2009).